Journal of Hydrology 525 (2015) 760–768

Contents lists available at ScienceDirect

Journal of Hydrology

journal homepage: www.elsevier.com/locate/jhydrol

Transport of *E. coli* D21g with runoff water under different solution chemistry conditions and surface slopes

Scott A. Bradford [a,*], Brendan Headd [a], Gilboa Arye [b], Jiří Šimůnek [c]

[a] US Salinity Laboratory, USDA, ARS, Riverside, CA, United States
[b] Jacob Blaustein Institutes for Desert Research, Ben-Gurion University of the Negev, Israel
[c] Department of Environmental Sciences, University of California, Riverside, CA, United States

ARTICLE INFO

Article history:
Received 13 August 2014
Received in revised form 20 January 2015
Accepted 20 April 2015
Available online 27 April 2015
This manuscript was handled by Laurent Charlet, Editor-in-Chief, with the assistance of Rizlan Bernier-Latmani, Associate Editor

Keywords:
Runoff
Solution chemistry
Slope
Microorganism
Modeling

SUMMARY

Tracer and indicator microbe runoff experiments were conducted to investigate the influence of solution chemistry on the transport, retention, and release of *Escherichia coli* D21g. Experiments were conducted in a chamber (2.25 m long, 0.15 m wide, and 0.16 m high) packed with ultrapure quartz sand (to a depth of 0.10 m) that was placed on a metal frame at slopes of 5.6%, 8.6%, or 11.8%. Runoff studies were initiated by adding a step pulse of salt tracer or D21g suspension at a steady flow rate to the top side of the chamber and then monitoring the runoff effluent concentrations. The runoff breakthrough curves (BTCs) were asymmetric and exhibited significant amounts of concentration tailing. The peak concentration levels were lower and the concentration tailing was higher with increasing chamber slope because of greater amounts of exchange with the sand and/or extents of physical nonequilibrium (e.g., water flow in rills and incomplete mixing) in the runoff layer. Lower amounts of tailing in the runoff BTC and enhanced D21g retention in the sand occurred when the solution ionic strength (IS) was 100 mM NaCl compared with 1 mM NaCl, due to compression of the double layer thickness which eliminated the energy barrier to attachment. Retained cells were slowly released to the runoff water when the IS of the runoff water was reduced to deionized water. The amount and rate of cell release was greatest at the highest chamber slope, which controlled the amount of exchange with the sand and/or the extent of physical nonequilibrium in the runoff layer, and the amount of retained cells. The observed runoff BTCs were well described using a transient storage model, but fitted parameters were not always physically realistic. A model that accounted for the full coupling between flow and transport in the runoff and sand layers provided useful information on exchange processes at the sand surface, but did not accurately describe the runoff BTCs which were influenced by physical nonequilibrium in the runoff layer.

Published by Elsevier B.V.

1. Introduction

Microorganism contamination of surface water resources is common in the United States (USEPA, 1997; Abbaszadegan et al., 2003; Borchardt et al., 2003), and has frequently been implicated in water- and food-borne disease outbreaks (Centers for Disease Control and Prevention, 1998; USFDA, 1998; Gerba and Smith, 2005; Pachepsky et al., 2011). High concentrations of pathogens, indicator microorganisms, and other colloids can be rapidly transported from agricultural fields, urban environments, and hillslopes to streams or locations of surface water storage by runoff water (Rahe et al., 1978; Heathwaite et al., 2005; Haygarth et al., 2006). Runoff has been reported to be the primary transport route for pathogen dissemination at the hillslope scale (Tyrrel and Quinton, 2003; Jamieson et al., 2004; Dorner et al., 2006). An understanding of processes that influence the transport of pathogens and indicator microorganisms in runoff water is therefore needed to assess and mitigate risks of microbial contamination of surface water supplies to human health.

As pathogens are transported with runoff water they undergo exchange with the soil surface. Exchange of solute and microorganisms to/from runoff water and the soil surface can be very complex, depending on advection, dispersion, and reactions (Bradford et al., 2013). In particular, advective exchange with the soil surface (infiltration and exfiltration) will depend on the surface water boundary conditions, the surface topography, the initial soil water status, hydraulic properties of the soil, soil structure, and subsurface

Abbreviations: DI, deionized; DLVO, Derjaguin–Landau–Verwey–Overbeek; IS, ionic strength.

* Corresponding author. Tel.: +1 951 369 4857.
E-mail address: Scott.Bradford@ars.usda.gov (S.A. Bradford).

http://dx.doi.org/10.1016/j.jhydrol.2015.04.038
0022-1694/Published by Elsevier B.V.

heterogeneity. Spatial and temporal variations in these factors can produce conditions of dynamic exchange between runoff water and the soil surface (Wörman et al., 2007). Depression and obstruction storage of surface water will also produce relatively immobile or stagnant zones of water connected to the mean runoff water. Such stagnant zones include pools and eddies along runoff channels, water isolated behind rocks, gravel or vegetation, or relatively inaccessible water due to uneven surface topography (Panday and Huyakorn, 2004). Diffusive exchange will occur between runoff water and such stagnant zones (Wallach and van Genuchten, 1990; Govindaraju, 1996; Wallach et al., 2001). Rain drop impact and erosion of contaminated soils and sediments are other mechanisms of pathogen exchange at the soil surface (Gao et al., 2004, 2005; Pachepsky and Shelton, 2011).

Pathogens at the soil surface may interact with soil particles and/or vegetation and become retained, and thereby diminish their transport with runoff water. A multitude of physical, chemical, and biological processes will influence the retention of microorganisms at the soil surface. For example, microbe retention in soil and sediment is known to depend on soil properties such as surface roughness, grain size and distribution, soil structure, mineralogy, and surface charge; properties of the water such as the water velocity, the water saturation, and the solution pH, ionic strength (IS), and composition; and properties of the microorganisms such as the size and surface charge, surface macromolecules, growth stage, motility, and biofilm (Ginn et al., 2002; Harvey and Harms, 2002; Foppen and Schijven, 2006; Tufenkji et al., 2006; Bradford et al., 2013). Temporal changes in these same factors may produce pathogen release. For example, a decrease in the solution IS will result in an expansion of the double layer thickness and an increase in the magnitude of the surface potential of the soil and microbe (Israelachvili, 1992; Elimelech et al., 1995) that will reduce the depth of the secondary minimum and promote microbe release (Lenhart and Saiers, 2003; Grolimund and Borkovec, 2006; Tosco et al., 2009; Bradford et al., 2012). Runoff water may subsequently become contaminated as a result of diffusion and exfiltration of released pathogens.

Most microbial runoff studies to date have examined the efficacy of vegetated buffer strips to remove pathogens (Atwill et al., 2002; Tate et al., 2004; Trask et al., 2004; Kouznetsov et al., 2007; Guber et al., 2007, 2009; Guzman et al., 2010; Fox et al., 2011; Wu et al., 2011; Yu et al., 2012, 2013). Wide variations in the removal efficiency of vegetative buffer strips have been reported in the literature (Fajardo et al., 2001; Koelsch et al., 2006; Mawdsley et al., 1995; Pachepsky et al., 2006; Tate et al., 2004); e.g., ranging from almost none to complete removal. This variability in performance is likely due to differences in design and operation of vegetative buffer strips, and incomplete characterization of factors influencing exchange with the soil surface. Fox et al. (2011) reported that *Escherichia coli* mass reductions in runoff water were highly correlated with the amount of water infiltration. However, only limited research has addressed the issue of microbial exchange between runoff water and the soil surface. Muirhead et al. (2006) reported that the transport behavior of a conservative tracer (bromide) and *E. coli* in runoff water was almost identical. Yu et al. (2011) reported similar results for kaolinite and bromide in runoff water. However, these studies did not consider the confounding effects of changes in solution chemistry on cell/kaolinite retention and release in the soil. Yu et al. (2013) reported greater retention of latex microspheres to surface vegetation occurred at higher IS and for larger particles. Ferguson et al. (2007) found that larger microorganisms (*Cryptosporidium* and *E. coli*) were more efficiently removed from runoff water than smaller microbes (coliphage PRD1) in field studies. Furthermore, previous studies have not yet modeled the full dynamics of water flow and microbial transport in runoff water and soil. Most modeling studies only consider runoff and transport at the soil surface, and approximate exchange between runoff water and the soil using simplified terms for infiltration and/or diffusive exchange (Guber et al., 2009; Yu et al., 2011, 2012; Wu et al., 2011; van Genuchten et al., 2013).

The objective of this research was to study the effects of slope and solution IS on the transport, exchange, retention, and release of an indicator microorganism (*E. coli* D21g) in runoff water. In particular, different amounts of advective exchange between the runoff water and the soil surface were achieved by varying the slope (5.6%, 8.6%, and 11.8%) of a chamber packed with fine sand. The IS of the runoff water was varied (1 and 100 mM NaCl) to obtain a wide range of cell retention and release (deionized water) conditions. Experiments were simulated using the transient storage model and a model that describes the full coupling of flow and transport (tracer and *E. coli* D21g) between runoff water and the sand in the chamber.

2. Materials and methods

2.1. Electrolyte solutions and porous media

Electrolyte solutions were prepared using deionized (DI) water (pH = 5.8) to achieve 0, 1, or 100 mM NaCl solutions. Ultrapure quartz sand (Iota Quartz, Unimin Corp. NC) was employed as a porous medium in the runoff experiments discussed below. The sand was thoroughly rinsed with DI water to eliminate background fines from the sand before use. The median grain size of this sand was measured to be 238 μm (standard deviation of 124 μm) with a laser scattering particle size and distribution analyzer (Horiba LA 930). The saturated conductivity (K_s) of the sand in a packed column was determined to be 0.57 cm min^{-1} using Darcy's law and measurements of the hydraulic gradient during steady-state water flow. The porosity of the packed column was calculated to be 0.44 from the measured bulk density (1.49 g cm^{-3}) and an assumed specific density of the sand (2.65 g cm^{-3}).

2.2. E. coli D21g

Experiments discussed below employed pure cultures of *E. coli* D21g, which is a gram-negative, nonmotile bacterial strain that produces minimal amounts of lipopolysaccharides and extra-cellular polymeric substances. *E. coli* D21g was grown 24 h before initiating experiments. A single colony of *E. coli* D21g was inoculated into 1000 mL of Luria–Bertani media containing 30 μg mL^{-1} gentamycin and incubated with shaking at 37 °C overnight. The bacterial suspension was centrifuged and rinsed three times before diluting the concentrated suspension into the desired electrolyte solution. Influent and effluent concentrations of *E. coli* D21g were determined using a spectrophotometer (Unico UV-2000, United Products & Instruments, Dayton, NJ) at a wavelength of 600 nm and a calibration curve. The average optical density at 600 nm for the influent cell suspension was 0.077, which corresponds to an input concentration (C_o) of approximately $1.1 * 10^6$ cells mL^{-1}.

2.3. Interaction energy calculations

The zeta potential of *E. coli* D21g and crushed ultrapure quartz sand in the various solution chemistries was determined from measured electrophoretic mobilities using a ZetaPALs instrument (Brookhaven Instruments Corporation, Holtsville, NY) and the Smoluchowski equation. The size of *E. coli* D21g in the various solution chemistries was measured using the laser scattering particle size and distribution analyzer. The total interaction energy of *E. coli* D21g upon approach to the quartz sand under the various

solution chemistries was calculated (Table 1) using Derjaguin–Landau–Verwey–Overbeek (DLVO) theory and a sphere-plate assumption (Derjaguin and Landau, 1941; Verwey and Overbeek, 1948). Electrostatic double layer interactions were quantified using the expression of Hogg et al. (1966) using zeta potentials in place of surface potentials. The retarded London-van der Waals attractive interaction force was determined from the expression of Gregory (1981). The value of the Hamaker constant used in these calculations was $6.5 * 10^{-21}$ J (Rijnaarts et al., 1995).

2.4. Runoff experiments

Fig. 1 presents a schematic of the setup used in the runoff studies. Experiments were conducted in a plexiglass chamber that was 2.25 m long, 0.15 m wide and 0.16 m high. Autoclaved ultrapure quartz sand was uniformly packed into the chamber to a depth of 0.1 m. The packed chamber was placed on a metal support frame at slopes of 5.6%, 8.6%, or 11.8%. Steady-state water flow was achieved in the chamber before initiating a transport experiment using a peristaltic pump (Barnant Company, Barrington, Illinois) connected to a rain simulator at the upslope portion of the chamber. The rain simulator consisted of a 13.2 cm diameter plexiglass disc that was continuously rotated to uniformly distribute solutions from the pump on one side of the chamber to a regular network of embedded syringe tips. The solutions were pumped at a constant water flux to slowly saturate the sand in the chamber, initiate steady-state runoff conditions, and to minimize soil erosion. The down slope portion of the chamber was equipped with a horizontal groove and fitting at the soil surface to continuously collect runoff water using a fraction collector.

Runoff experiments were conducted to determine the influence of solution chemistry on D21g transport and removal from runoff water. Table 2 provides a summary of the applied flow rates. A step pulse of microbial suspension was pumped into the chamber for 30 min (Phase 1). Next, eluting solution was pumped to the chamber for 90 min (Phase 2). The initial resident solution, D21g suspension, and eluting solutions had the same solution chemistry during a given experiment. Two solution chemistries at pH = 5.8 were considered, namely: (i) 1 mM NaCl; and (ii) 100 mM NaCl. Retention of D21g in the 1 mM NaCl was highly unfavorable (a large energy barrier), whereas conditions were much more favorable (no energy barrier) for deposition in 100 mM NaCl (Table 1). An additional elution with DI water for 120 min (Phase 3) occurred in some experiments to examine the potential of D21g release after expansion of the double layer thickness and reduction of the secondary minimum. Collected effluent water samples were analyzed for D21g concentrations as described above. A mass balance in the runoff water was conducted based on information on the water flow rate and D21g concentrations in the influent and runoff effluent. All runoff experiments (Phases 1 and 2) were replicated and exhibited good reproducibility.

Following completion of a runoff experiment, the chamber was lowered to a horizontal position and DI water was pumped into the chamber from below through five valves located along the length of the chamber bottom. The chamber was then drained and the process was repeated at least six times. Sand samples obtained from four different depths (from the surface to a maximum depth of 10 cm) showed no evidence of D21g growth. In addition, the optical density readings of runoff effluent prior to D21g injection were consistently at or near zero. Taken together, these data indicated that background D21g interference was negligible using this procedure, and this eliminated the need to repack the large volume of sand in the chamber each time.

Replicate salt tracer (100 mM NaCl) experiments were conducted for each chamber slope using a similar protocol as for the D21g runoff experiments described above. In this case, the runoff chamber was initially saturated with DI water and then sequentially eluted with 100 mM NaCl (30 min) and DI water (90 min). Changes in the electrical conductivity (EC) of the effluent runoff samples were measured using a CS547A water conductivity probe and a CR10X data logger (Campbell Scientific, Logan, UT).

Table 1
Zeta potentials and DLVO interaction energy parameters.

Ionic strength (mM)	Sand zeta potential (mV)	D21g zeta potential (mV)	Energy barrier (kT)	Depth of secondary energy minimum (kT)
1	−66.8	−53.5	3270	0.0
25	−31.8	−29.3	494	−3.6
100	−25.5	−11.6	NB	NA

NB – No barrier to attachment.
NA – Not applicable.
kT – normalized by the product of the Boltzmann constant and the absolute temperature.

2.5. Transient storage model

The transient storage model has commonly been employed to simulate the transport of solutes in surface water (Thackston and Schnelle, 1970; Bencala and Walters, 1983; LeGrand-Marcq and Laudelout, 1985; Runkel et al., 1996; Choi et al., 2000; De Smedt, 2006). The transient storage model considers advective and dispersive transport in the runoff layer, and diffusive exchange with water in stagnant zones (e.g., the soil) using a quasi steady-state approximation of Fick's first law of diffusion as:

$$\frac{\partial C_m}{\partial t} = D\frac{\partial^2 C_m}{\partial x^2} - v_w\frac{\partial C_m}{\partial x} - \alpha(C_m - C_{im}) \quad (1)$$

$$\frac{\partial C_{im}}{\partial t} = \alpha\frac{A_m}{A_{im}}(C_m - C_{im}) \quad (2)$$

where C_m [$N_c L^{-3}$; N_c and L denotes the number of cells and length, respectively] is the cell concentration in the mobile runoff water, C_{im} [$N_c L^{-3}$] is the cell concentration in the immobile storage zone, D [$L^2 T^{-1}$; T denotes units of time] is the longitudinal hydrodynamic dispersion coefficient, v_w [$L T^{-1}$] is the longitudinal runoff water velocity, x [L] is the longitudinal coordinate, t [T] is the time, A_m [L^2] is the cross sectional area of the runoff water, A_{im} [L^2] is the cross section area of the storage zone, and α [T^{-1}] is the mass transfer coefficient to/from the runoff water and storage zone. Note that $A_m = wh_m$ and $A_{im} = wh_{im}$, where w [L] is the width of the runoff chamber, h_m [L] is the height of the runoff water, and h_{im} [L] is the depth of the storage zone. The total height (h_T, L) in runoff and storage zones is $h_T = h_m + h_{im}$. The value of v_w is equal to Q/A_m; where Q [$L^3 T^{-1}$] is the runoff water flux.

The transient storage model is mathematically equivalent to the mobile-immobile model (van Genuchten et al., 2013), denoted below as MIM. In this case, the MIM is derived from Eqs. (1) and (2) by replacing h_m and h_{im} with the water contents in the mobile (θ_m) and immobile (θ_{im}) regions, respectively, h_T is replaced by the total porosity (θ), v_w is defined as the ratio of the Darcy water velocity (q_w) and θ_m, and α is replaced by α_m/θ_m; where α_m [T^{-1}] is the mass exchange coefficient between mobile and immobile regions. The Hydrus-1D software (Šimůnek et al., 2008) was used to numerically solve Eqs. (1) and (2), and to determine model parameters (h_T, h_{im}, and α) by inverse optimization to measured breakthrough curves (BTCs) in the runoff effluent using a nonlinear least squares routine (Marquardt, 1963).

2.6. Fully coupled model

Recent research has demonstrated that flow and transport in runoff water can be simulated using similar equations to those

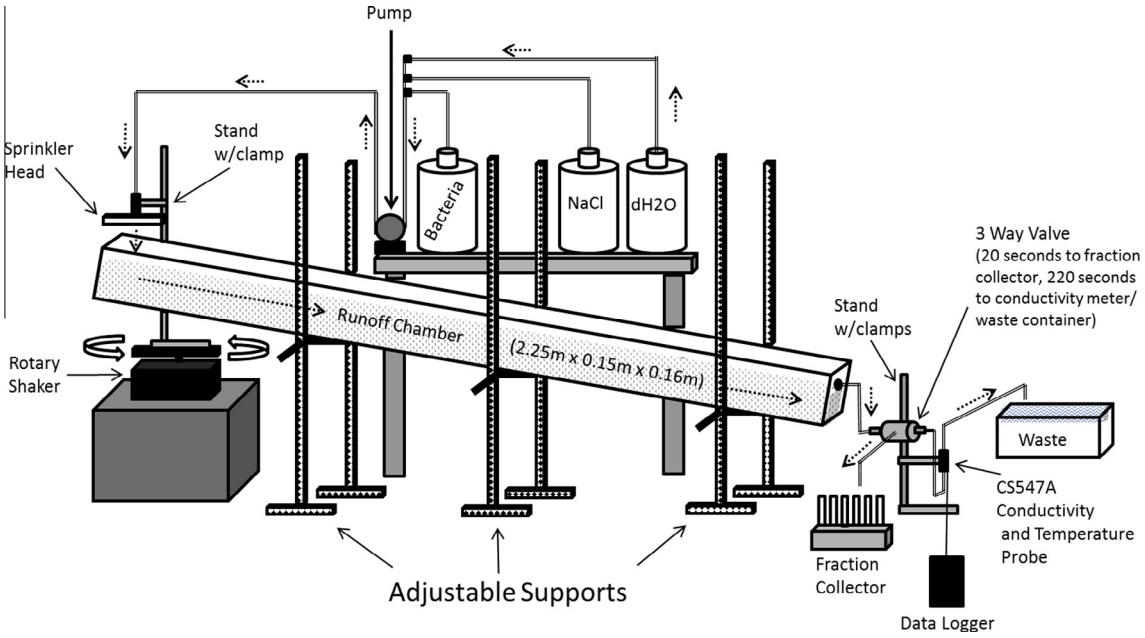

Fig. 1. A schematic of the setup used in the runoff studies.

Table 2
A summary of experimental conditions and transient storage model parameters.

	IS (mM)	Slope (%)	Q (mL min^{-1})	h_T (cm)	h_{im} (cm)	h_m (cm)	α (min^{-1})	R^2
Tracer	100	5.6	122	1.01	0.94	0.06	0.20	0.99
Tracer	100	8.6	122	1.00	0.93	0.07	0.28	0.99
Tracer	100	11.8	124	1.25	1.16	0.09	0.38	0.97
D21g	1	5.6	126	1.18	1.11	0.07	0.19	0.97
D21g	1	8.6	126	1.01	0.93	0.07	0.36	0.98
D21g	1	11.8	150	1.54	1.46	0.08	0.52	0.90
D21g	100	5.6	131	1.14	1.07	0.07	0.23	0.99
D21g	100	8.6	123	1.27	1.22	0.04	0.54	0.95
D21g	100	11.8	131	3.09	3.00	0.09	0.41	0.90

used in the subsurface (Richards' and advective dispersion equations, respectively) when using appropriate functions of the hydraulic conductivity, the capacitance, and the water content at the soil surface (Weill et al., 2009; Bittelli et al., 2010). These hydraulic property modifications are especially simple under saturated, steady-water flow conditions when a constant value of porosity and K_s are employed in the runoff layer. This finding implies that it may be feasible to use existing subsurface simulation routines to model fully coupled flow and transport in the runoff water and the subsurface. In this work, we employ the finite element HYDRUS (2D/3D) model (Šimůnek et al., 2011) to simulate water flow and transport in the runoff chamber.

The runoff chamber was modeled using runoff (top 2 cm) and sand (bottom 10 cm) layers parallel to the chamber slope with different soil hydraulic properties. Water flow in the chamber was simulated using the solution of Richards' equation (Richards, 1931):

$$\frac{\partial \theta}{\partial t} = \frac{\partial}{\partial x_i}\left(K_{ij}(\theta)\frac{\partial h}{\partial x_j} + K_{iz}(\theta)\right) \quad (3)$$

where x_i (i = 1, 2) are the spatial coordinates [L], θ [L^3 L^{-3}] is the volumetric water content, K_{ij} [L T^{-1}] are components of the hydraulic conductivity tensor, and h [L] is the pressure head.

Transport of a conservative tracer was simulated using an advection–dispersion equation (ADE):

$$\frac{\partial(\theta C)}{\partial t} = \frac{\partial}{\partial x_i}\left(\theta D_{ij}\frac{\partial C}{\partial x_j}\right) - \frac{\partial q_i C}{\partial x_i} \quad (4)$$

where C [M L^{-3}, where M denotes units of mass] is the tracer concentration in the aqueous phase, D_{ij} [L^2 T^{-1}] is the hydrodynamic dispersion tensor, and q_i [L T^{-1}] is the Darcy water velocity in the i direction.

Constant water flux boundary conditions were imposed at the upslope boundary of the runoff layer, and a seepage face was maintained at the downslope boundary of the runoff layer. No flow boundary conditions were imposed on all other exterior surfaces of the sand and runoff layers. A third-type boundary condition was used at the inlet, and at the runoff chamber seepage face outlet.

As discussed above, the porosity of the sand in the chamber was determined directly from measurements of steady-state water flow in a saturated packed column. Values of K_s in the runoff layer and the sand were estimated by inverse optimization to the runoff BTC for the salt tracer. Other unsaturated hydraulic properties for the sand were taken from Jacobson et al. (2009). The longitudinal dispersivity (λ_L) in the sand and runoff layers was taken as 0.1 of the chamber length (Gelhar et al., 1985, 1992). The transverse dispersivity (λ_T) was taken to be $0.1 * \lambda_L$ in both layers.

3. Results and discussion

3.1. DLVO calculations

Table 1 presents information on the zeta potentials of D21g and quartz sand, and the DLVO energy barrier height and the depth of the secondary minimum for D21g-quartz sand interactions under the various solution chemistry conditions. The median size of D21g was determined to be 1.46 μm (the standard deviation was 0.57) in the various solution chemistries. The energy barrier height decreased and the secondary minimum increased with increasing IS. Conditions were highly unfavorable for D21g attachment when the IS $\leqslant$ 1 mM NaCl. Conversely, retention of D21g in association with a primary minimum is possible when the IS = 100 mM NaCl.

3.2. Runoff experiments

Fig. 2 presents BTCs for a 100 mM NaCl tracer when the runoff chamber slope was 5.6%, 8.6%, and 11.8%. All of the BTCs exhibited

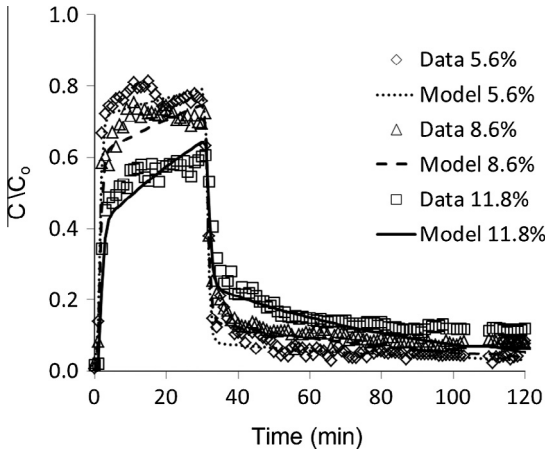

Fig. 2. Observed and simulated runoff breakthrough curves for a 100 mM NaCl tracer when the runoff chamber slope was 5.6%, 8.6%, and 11.8%. The simulations where obtained using the transient storage model (Eqs. (1) and (2)). Fitted model parameters are given in Table 2.

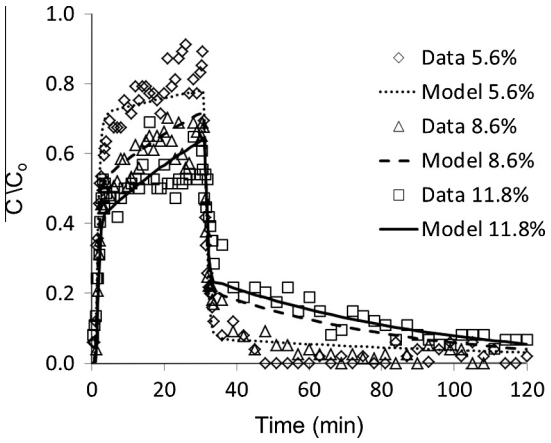

Fig. 3. Observed and simulated runoff breakthrough curves for D21g in 1 mM NaCl solution when the runoff chamber slope was 5.6%, 8.6%, and 11.8%. The simulations where obtained using the transient storage model (Eqs. (1) and (2)). Fitted model parameters are given in Table 2.

an initially high pulse of tracer in the runoff effluent followed by prolonged tailing at lower concentration levels. The initial pulse in the BTC reflects rapid transport of the tracer in the runoff water. The height of this pulse and the tailing behavior of the BTC depends on: (i) the amount of exchange at the surface of the sand layer due to infiltration, exfiltration, and diffusion; and/or (ii) the extent of physical nonequilibrium transport in the runoff layer due to flow in small rivulets and incomplete mixing. Higher chamber slopes produce lower breakthrough concentrations initially and then higher levels of concentration tailing. This observation indicates that higher slopes produced greater amounts of exchange with the sand and/or extents of physical nonequilibrium in the runoff layer. Each of these explanations will be discussed in detail later.

Fig. 3 presents BTCs in the runoff effluent for D21g when the chamber slope was 5.6%, 8.6%, and 11.8% and the IS = 1 mM NaCl. In this case, the peak effluent concentrations and the concentration tailing behavior for D21g were quite similar to the 100 mM NaCl tracer results shown in Fig. 2. Similar to the tracer, the runoff BTC height decreased and the amount of tailing increased for D21g with the chamber slope. These results indicate that minimal amounts of D21g retention occurred in the chamber sand when the solution IS was 1 mM NaCl, and that differences in the BTC shape were again due to the amount of exchange and/or the extent of physical nonequilibrium in the runoff layer. Little D21g retention is expected in the sand when the IS = 1 mM because of the larger energy barrier and the minor depth of the secondary minimum (Table 1). Tracer and colloid (*E. coli* and kaolinite clay) transport in runoff water have previously been reported to be nearly identical (Muirhead et al., 2006; Yu et al., 2011).

Fig. 4 presents similar information to Fig. 3, but for D21g in 100 mM NaCl. Greater amounts of D21g retention are expected in the sand when the IS = 100 (Fig. 4) than 1 mM NaCl (Fig. 3) because the energy barrier to attachment was eliminated (Table 1). An estimate of the amount of cell retention was obtained from the difference in the effluent mass balance for the tracer and D21g in 100 mM solution to be 0.07, 0.16, and 0.35 when the chamber slope was 5.6%, 8.6%, and 11.8%, respectively. This observed increase in cell retention with chamber slope reflects an increasing influence of exchange with the sand. Comparison of Figs. 2 and 4 reveals that cell retention in the sand tended to lower the peak height of the runoff BTC compared to the tracer, especially as the chamber slope increased. Interestingly, cell retention also eliminated most of the tailing portion of the runoff BTCs that was observed for the tracer. Consequently, the influence of

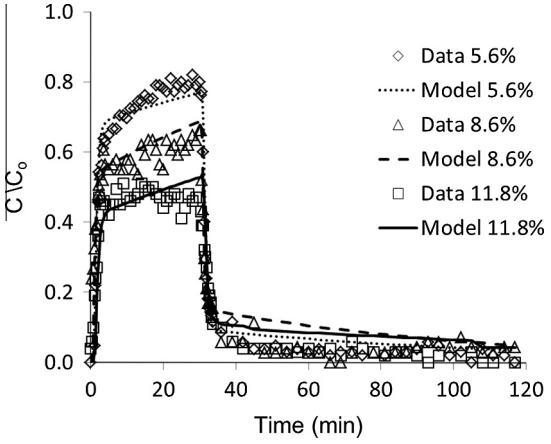

Fig. 4. Observed and simulated runoff breakthrough curves for D21g in 100 mM NaCl solution when the runoff chamber slope was 5.6%, 8.6%, and 11.8%. The simulations where obtained using the transient storage model (Eqs. (1) and (2)). Fitted model parameters are given in Table 2.

exchange and/or physical nonequilibrium on the tailing portion of the runoff BTC was partially masked by bacteria retention in the sand. This implies that reactive transport processes in runoff water may potentially be misinterpreted without complimentary information on conservative tracers.

The release and transport behavior of D21g cells were subsequently investigated during Phase 3 when the runoff solution IS was reduced from 100 mM NaCl to DI water. This change in IS expands the double layer thickness and can eliminate some primary minimum interactions that contribute to cell retention when the effects of surface roughness and Born repulsion are considered in interaction energy calculations (Bradford and Torkzaban, 2013). Fig. 5 presents observed release curves for D21g in the runoff effluent for the various chamber slopes. Cell release and transport occurs when the IS was reduced in the sand. Subsequently, diffusion, hydrodynamic dispersion, and exfiltration contribute to the slow transfer of cells from the sand to runoff water. The effluent mass balance on cell release was 0.0, 0.14, and 0.24 when the chamber slope was 5.6%, 8.6%, and 11.8%, respectively. These results demonstrate that the amount of cell release was strongly related to the chamber slope. The chamber slope determines the quantity of exchange and/or the extent of physical nonequilibrium in the runoff layer (Fig. 2), and this subsequently impacts the

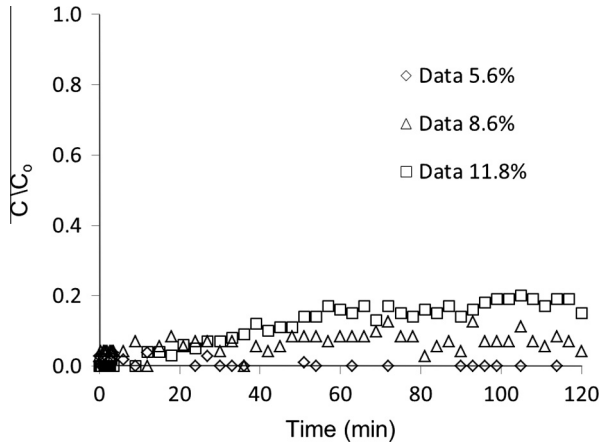

Fig. 5. Observed release curves for D21g when the runoff chamber slope was 5.6%, 8.6%, and 11.8%. Release was initiated during Phase 3 by switching the influent solution IS from 100 to 0 mM NaCl.

amount of retention in the sand (Fig. 4). Consequently, differences in cell release with chamber slope mainly reflect the initial amount of cell retention in the sand when the IS = 100 mM NaCl solution and the amount of exchange and/or the extent of physical nonequilibrium in the runoff layer.

3.3. Transient storage model

Figs. 2–4 also present simulated tracer and D21g BTCs in the runoff effluent when the chamber slope was 5.6%, 8.6%, and 11.8%. Simulations were obtained using the solution of Eqs. (1) and (2). Table 2 provides a summary of the experimental (IS, Q, slope), fitted (h_T, h_{im}, and α), and calculated (h_m) model parameters and the Pearson's correlation coefficient (R^2) values. In general the model provided a reasonable description of the experimental data ($R^2 > 0.90$). Calculated values of $h_m = h_T - h_{im}$ were always less than 0.09 cm, reflecting the small height of the water in the runoff layer. In contrast, values of h_{im} were always much larger (1–3.09 cm) than h_m, and provided an indication of the depth of the storage zone in the sand that contributed to exchange and/or the extent of physical nonequilibrium in the runoff layer. The amount of exchange with the sand and/or the extent of physical nonequilibrium in the runoff water layer depended on the values of h_T, h_{im}, and α. In general, values of h_T, h_{im}, and α tended to increase with increasing chamber slope because of enhanced exchange and/or physical nonequilibrium. The increase in α with increasing slope indicates a greater rate of diffusive mass transfer between the runoff water and the stagnant zone.

Even though the transient storage model provides a reasonable fit of the experimental data, the fitted model parameters were not always realistic. For example, the Manning equation of overland flow predicts that the value of h_m should decrease with the chamber slope, whereas the opposite trend was sometimes observed (Table 2). Furthermore, values of α were high (ranging from 0.19 to 0.54 min^{-1}), which were not consistent with a slow diffusion controlled exchange process. In addition, the transient storage model sometimes did not fully capture the tailing behavior in the runoff BTCs (Figs. 3 and 4). Advective exchange between the runoff layer and the subsurface was not considered in the transient storage model because of steady-state water flow conditions in the chamber. Consequently, the transient storage model does not account for important exchange processes in the sand, such as infiltration, transport, retention, release, and exfiltration.

3.4. Fully coupled model

To improve our understanding of the runoff transport and exchange processes for the tracer we employed a model that accounted for the full coupling between runoff water and the subsurface. Fig. 6 shows the cumulative amount of tracer that crosses the total surface of the sand layer (Fig. 6a), and the top (Fig. 6b), middle (Fig. 6c), and bottom (Fig. 6d) third of the surface of the sand layer as a function of time when the chamber slope was 5.6%, 8.6%, and 11.8%. Simulation results indicate that tracer exchange with the sand layer was dominated by advection which varied with the slope and the distance along the slope. Infiltration occurred mainly upslope, and initially served as a sink for the tracer (negative values), whereas exfiltration mainly occurred downslope and it served as a delayed tracer source to the runoff layer. The contribution of infiltration and exfiltration on the runoff BTC depended on the chamber slope and the transport of the tracer through the sand layer downslope. Indeed, higher slopes (elevations) increase the influence of gravity on water flow, which tended to produce greater infiltration upslope and transport of the tracer to deeper depths in the sand. Consequently, infiltration and exfiltration played an important role in exchange between runoff water and the sand layer at higher slopes, and were partially responsible for the observed differences in the runoff BTC shapes shown in Fig. 2.

The use of the fully coupled model to study exchange process at the interface of runoff water and the sand surface has some significant advantages over the transient storage model. Exchange processes between runoff water and the surface of natural soils are complex, and are expected to depend on the surface topography, obstruction and depression storage, the initial soil water status, soil hydraulic properties, subsurface heterogeneity, and preferential flow pathways (Bradford et al., 2013). The roles of advective and diffusive exchange across the soil surface are likely to change with these surface and soil properties, and the use of the fully coupled model is potentially an important tool to help understand the influence of these various factors. However, use of the fully coupled model requires knowledge of many additional parameter values (e.g., conductivities and dispersivities in the sand and runoff layers) than the transient storage model.

A more significant limitation of the transient storage and fully coupled models arises from the conceptual description of water flow in the runoff layer. In particular, water flow in the runoff layer is implicitly assumed in diffusion and kinematic wave equations to occur as sheet flow; e.g., a thin, continuous film over the smooth soil surface. In reality, erosion at the soil surface is complex, and is well known to produce concentrated water flow and transport in rills and rivulets (Dunne et al., 1991; Darboux and Huang, 2005; Thompson et al., 2010). Similarly, we observed enhanced water flow in small rivulets in our runoff chamber experiments. This deviation from sheet flow can produce preferential flow pathways and incomplete mixing of the tracer in the runoff layer. Both of these factors are presently not accounted for in the fully coupled model, and may produce significant deviations in observed and simulated transport. For example, Fig. 7 presents observed and simulated tracer BTCs in the runoff effluent when the chamber slope was 11.8%. Note that the fully coupled model overestimates the arrival time of the runoff BTC, and underestimates the amount of concentration tailing. These observations suggest that physical nonequilibrium flow and transport processes were significantly contributing to behavior in the runoff layer as a result of nonuniform water flow and incomplete mixing, and that transport models need to account for such processes. We did not attempt to simulate the transport, retention, and release of D21g in the chamber experiments using the fully coupled model due to this limitation. It should be mentioned that a number of flow and transport models

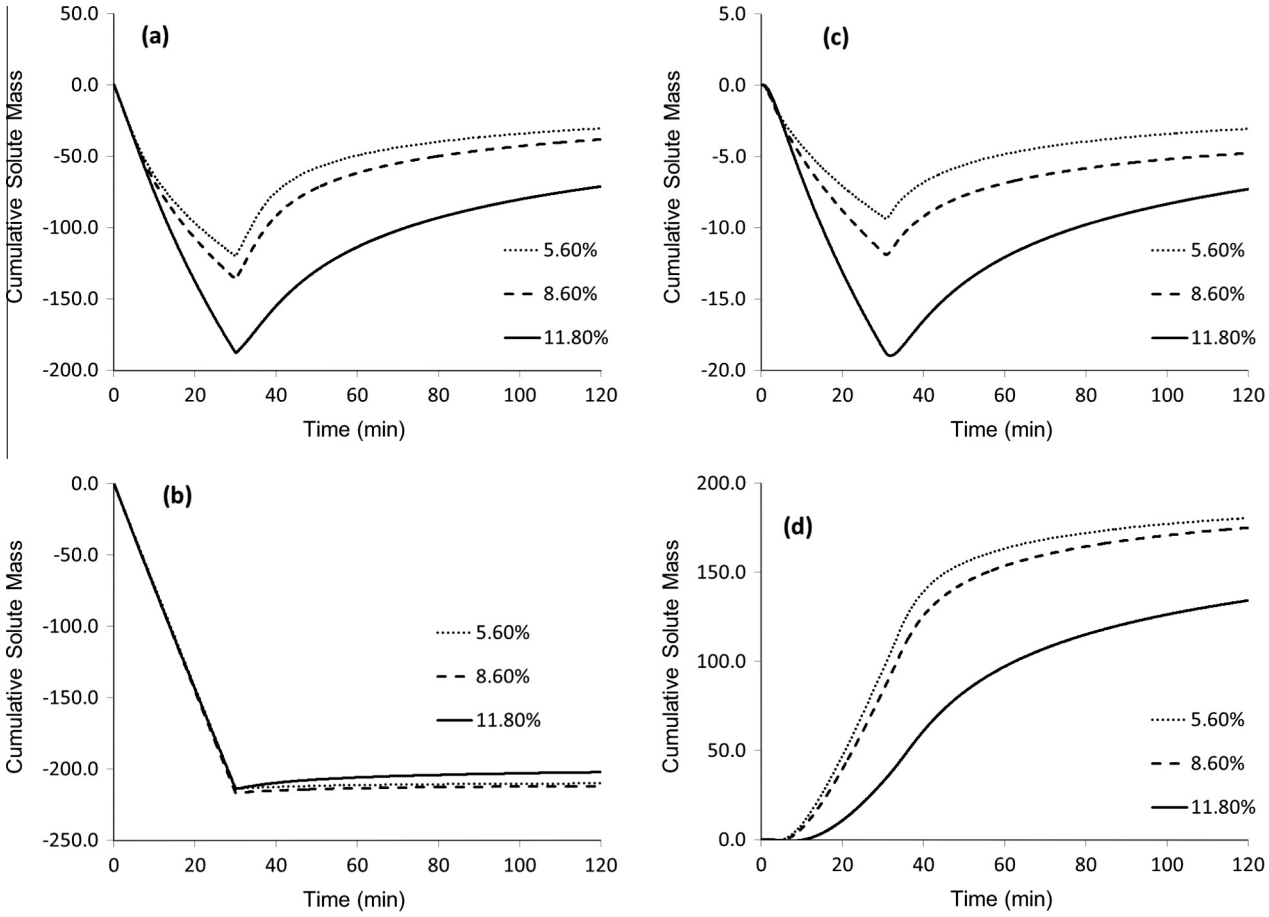

Fig. 6. The simulated cumulative amount of tracer mass that is transferred across the total sand surface (a), the top third of the sand surface (b), the middle third of the sand surface (c), and the bottom third of the sand surface (d) when the chamber slope was 5.6%, 8.6%, and 11.8%. A negative mass indicates that the tracer has moved into the sand, and a positive mass indicates that the tracer has entered the runoff layer.

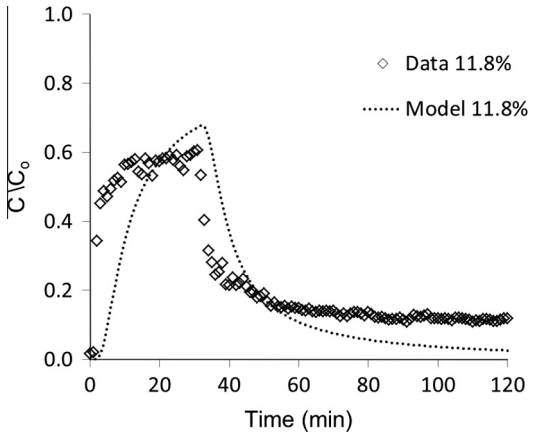

Fig. 7. Observed and simulated runoff breakthrough curves for a 100 mM NaCl tracer when the runoff chamber slope was 11.8%. The simulations where obtained using the fully coupled model (Eqs. (3) and (4)) and fitted values of $K_s = 0.108$ and 6000 cm min^{-1} for the sand and runoff layers, respectively.

have been developed to describe physical nonequilibrium processes in porous media (e.g., Jarvis, 2007; Šimůnek and van Genuchten, 2008; Köhne et al., 2009). It is possible that these models may be extended to account for similar physical nonequilibrium processes in the runoff layer, but such an undertaking is beyond the scope of this paper.

4. Summary and conclusions

Experimental and numerical modeling studies were initiated to study the effects of solution IS and chamber slope on the transport, retention, and release of *E. coli* D21g in runoff water. Complimentary conservative tracer studies revealed the importance of exchange with the sand and/or physical nonequilibrium in the runoff layer. In particular, the peak effluent concentration and the amount of concentration tailing in the runoff BTC were strongly dependent on the amount of water infiltration and exfiltration. Lower peak concentrations and greater amounts of concentration tailing in the runoff BTC were associated with greater amounts of infiltration, exfiltration, and physical nonequilibrium (e.g., flow in small rivulets and incomplete mixing) that occurred with increasing runoff chamber slope. Infiltration primarily occurred upslope, whereas exfiltration mainly happened downslope.

In addition to infiltration and exfiltration, the transport of *E. coli* D21g was also sensitive to the solution IS because of its influence on cell retention. The runoff BTC for D21g was very similar to that of the conservative tracer when the IS was low (1 mM NaCl) because cell retention was highly unfavorable. In this case, the amount of infiltration, exfiltration, and physical nonequilibrium controlled the runoff BTC shape. Conversely, cell retention in the sand increased under high IS (100 mM NaCl) conditions due to elimination of the energy barrier to attachment. Enhanced cell retention tended to lower the peak effluent concentration and to drastically reduce the amount of concentration tailing in the runoff

BTC of D21g in comparison to the conservative tracer. Consequently, cell retention may mask the influence of various exchange and/or physical nonequilibrium processes that occur at the interface of runoff water and soil.

Retained cells could be released back into the runoff water when the IS of the runoff water was decreased and the diffuse double layer was expanded. The amount and rate of cell release from the sand layer depended upon the initial distribution of retained cells, the amounts of infiltration and exfiltration (the chamber slope), the rate of transport through the sand layer, and the extent of physical nonequilibrium.

The transient storage model is commonly used to describe transport and diffusive exchange of solutes and microbes in runoff water. This model provided a good description of the runoff BTCs, but model parameters were not always physically realistic. Simulations from a fully coupled flow and transport model provided valuable insight on advective and diffusive exchange processes at the interface of runoff water and the sand surface. However, the coupled model did not provide an adequate description of the runoff BTCs. This discrepancy, and experimental evidence (e.g., flow in small rivulets), indicates that physical nonequilibrium processes were occurring in the runoff layer and that the model assumption of sheet flow was violated.

Acknowledgments

This research was supported by the 214 Manure and Byproduct Utilization Project of the USDA–ARS. Mention of trade names and company names in this manuscript does not imply any endorsement or preferential treatment by the USDA.

References

Abbaszadegan, M., LeChevallier, M.W., Gerba, C.P., 2003. Occurrence of viruses in US groundwaters. J. Am. Water Works Assoc. 95, 107–120.
Atwill, E.R., Hou, L., Karle, B.M., Harter, T., Tate, K.W., Dahlgren, R.A., 2002. Transport of Cryptosporidium Parvum oocysts through vegetated buffer strips and estimated filtration efficiency. Appl. Environ. Microbiol. 68, 5517–5527.
Bencala, K., Walters, R., 1983. Simulation of transport in a mountain pool-and-riffle stream: a transient storage model. Water Resour. Res. 19, 718–724.
Bittelli, M., Tomei, F., Pistocchi, A., Flury, M., Boll, J., Brooks, E.S., Antolini, G., 2010. Development and testing of a physically based, three-dimensional model of surface and subsurface hydrology. Adv. Water Resour. 33, 106–122.
Borchardt, M.A., Bertz, P.D., Spencer, S.K., Battigelli, D.A., 2003. Incidence of enteric viruses in groundwater from household wells in Wisconsin. Appl. Environ. Microbiol. 69, 1172–1180.
Bradford, S.A., Torkzaban, S., 2013. Colloid interaction energies for physically and chemically heterogeneous porous media. Langmuir 29, 3668–3676.
Bradford, S.A., Torkzaban, S., Kim, H., Simunek, J., 2012. Modeling colloid and microorganism transport and release with transients in solution ionic strength. Water Resour. Res. 48, W09509. http://dx.doi.org/10.1029/2012WR012468.
Bradford, S.A., Morales, V.L., Zhang, W., Harvey, R.W., Packman, A.I., Mohanram, A., Welty, C., 2013. Transport and fate of microbial pathogens in agricultural settings. Crit. Rev. Environ. Sci. Technol. 43, 775–893.
Centers for Disease Control and Prevention, 1998. Surveys of Waterborne Disease Outbreaks Compiled by the Center for Disease Control and Prevention from 1986 to 1998. Centers for Disease Control and Prevention, Atlanta, GA.
Choi, J., Harvey, J.W., Conklin, M.H., 2000. Characterizing multiple timescales of stream and storage zone interaction that affect solute fate and transport in streams. Water Resour. Res. 36, 1511–1518.
Darboux, F., Huang, C.H., 2005. Does soil surface roughness increase or decrease water and particle transfers? Soil Sci. Soc. Am. J. 69, 748–756.
De Smedt, F., 2006. Analytical solution for transport of decaying solutes in rivers with transient storage. J. Hydrol. 330, 672–680.
Derjaguin, B., Landau, L., 1941. Theory of the stability of strongly charged lyophobic sols and of the adhesion of strongly charged particles in solutions of electrolytes. Acta Physicochim. URSS 14, 633–662.
Dorner, S.M., Anderson, W.B., Slawson, R.M., Kouwen, N., Huck, P.M., 2006. Hydrologic modeling of pathogen fate and transport. Environ. Sci. Technol. 40, 4746–4753.
Dunne, T., Zhang, W., Aubry, B.F., 1991. Effects of rainfall, vegetation, and microtopography on infiltration and runoff. Water Resour. Res. 27, 2271–2285.
Elimelech, M., Gregory, J., Jia, X., Williams, R.A., 1995. Particle Deposition and Aggregation: Measurement, Modeling, and Simulation. Butterworth-Heinemann, Oxford, England.
Fajardo, J.J., Bauder, J.W., Cash, S.D., 2001. Managing nitrate and bacteria in runoff from livestock confinement areas with vegetative filter strips. J. Soil Water Conserv. 56, 185–191.
Ferguson, C., Davies, C., Kaucner, C., Ashbolt, N., Krogh, M., Rodehutskors, J., Deere, D., 2007. Field scale quantification of microbial transport from bovine faeces under simulated rainfall events. J. Water Health 5, 83–95.
Foppen, J.W.A., Schijven, J.F., 2006. Evaluation of data from the literature on the transport and survival of *Escherichia coli* and thermotolerant coliforms in aquifers under saturated conditions. Water Res. 40, 401–426.
Fox, G.A., Matlock, E.M., Guzman, J.A., Sahoo, D., Stunkel, K.B., 2011. Load reduction from runoff by vegetative filter strips: a laboratory-scale study. J. Environ. Qual. 40, 980–988.
Gao, B., Walter, M.T., Steenhuis, T.S., Hogarth, W.L., Parlange, J.Y., 2004. Rainfall induced chemical transport from soil to runoff: theory and experiments. J. Hydrol. 295, 291–304.
Gao, B., Walter, M.T., Steenhuis, T.S., Parlange, J.Y., Richards, B.K., Hogarth, W.L., Rose, C.W., 2005. Investigating raindrop effects on transport of sediment and non-sorbed chemicals from soil to surface runoff. J. Hydrol. 308, 313–320.
Gelhar, L.W., Mantaglou, A., Welty, C., Rehfeldt, K.R., 1985. A review of field scale physical solute transport processes in unsaturated and saturated porous media. In: EPRI Topical Report EA-4190, Electric Power Research Institute, Palo Alto, CA.
Gelhar, L.W., Welty, C., Rehfeldt, K.R., 1992. A critical review of data on field-scale dispersion in aquifers. Water Resour. Res. 28, 1955–1974.
Gerba, C.P., Smith Jr., J.E., 2005. Sources of pathogenic microorganisms and their fate during land application of wastes. J. Environ. Qual. 34, 42–48.
Ginn, T.R., Wood, B.D., Nelson, K.E., Scheibe, T.D., Murphy, E.M., Clement, T.P., 2002. Processes in microbial transport in the natural subsurface. Adv. Water Resour. 25, 1017–1042.
Govindaraju, R.S., 1996. Modeling overland flow contamination by chemicals mixed in shallow soil horizons under variable source area hydrology. Water Resour. Res. 32, 753–758.
Gregory, J., 1981. Approximate expression for retarded van der Waals interaction. J. Colloid Interf. Sci. 83, 138–145.
Grolimund, D., Borkovec, M., 2006. Release of colloidal particles in natural porous media by monovalent and divalent cations. J. Contam. Hydrol. 87, 155–175.
Guber, A.K., Karns, J.S., Pachepsky, Y.A., Sadeghi, A.M., Van Kessel, J.S., Dao, T.H., 2007. Comparison of release and transport of manure-borne *Escherichia coli* and enterococci under grass buffer conditions. Lett. Appl. Microbiol. 44, 161–167.
Guber, A.K., Yakirevich, A.M., Sadeghi, A.M., Pachepsky, Y.A., Shelton, D.R., 2009. Uncertainty evaluation of coliform bacteria removal from vegetated filter strip under overland flow condition. J. Environ. Qual. 38, 1636–1644.
Guzman, J.A., Fox, G.A., Payne, J.B., 2010. Surface runoff transport of *Escherichia coli* after poultry litter application on pastureland. Trans. ASABE 53, 779–786.
Harvey, R.W., Harms, H., 2002. Transport of microorganisms in the terrestrial subsurface: in situ and laboratory methods. In: Hurst, C.J., Knudsen, G.R., McInerney, M.J., Stetzenback, L.D., Crawford, R.L. (Eds.), In Manual of Environmental Microbiology. ASM Press, Washington, DC, pp. 753–776.
Haygarth, P.M., Bilotta, G.S., Bol, R., Brazier, R.E., Butler, P.J., Freer, J., Gimbert, L.J., Granger, S.J., Krueger, T., Macleod, C.J.A., Naden, P., Old, G., Quinton, J.N., Smith, B., Worsfold, P., 2006. Processes affecting transfer of sediment and colloids, with associated phosphorus, from intensively farmed grasslands: an overview of key issues. Hydrol. Process. 20, 4407–4413.
Heathwaite, L., Haygarth, P., Matthews, R., Preedy, N., Butler, P., 2005. Evaluating colloidal phosphorus delivery to surface waters from diffuse agricultural sources. J. Environ. Qual. 34, 287–298.
Hogg, R., Healy, T.W., Fuerstenau, D.W., 1966. Mutual coagulation of colloidal dispersions. Trans. Faraday Soc. 62, 1638–1651.
Israelachvili, J.N., 1992. Intermolecular and Surface Forces. Academic Press, San Diego, CA.
Jacobson, K.H., Lee, S., McKenzie, D., Benson, C.H., Pedersen, J.A., 2009. Transport of the pathogenic prion protein through landfill materials. Environ. Sci. Technol. 43, 2022–2028.
Jamieson, R., Gordon, R., Joy, D., Lee, H., 2004. Assessing microbial pollution of rural surface waters: a review of current watershed scale modeling approaches. Agric. Water Manage. 70, 1–17.
Jarvis, N.J., 2007. Review of non-equilibrium water flow and solute transport in soil macropores: principles, controlling factors and consequences for water quality. Eur. J. Soil Sci. 58, 523–546.
Koelsch, R.K., Lorimor, J.C., Mankin, K.R., 2006. Vegetative treatment systems for management of open lot runoff: review of literature. Appl. Eng. Agric. 22, 141–153.
Köhne, J.M., Köhne, S., Šimůnek, J., 2009. A review of model applications for structured soils: a water flow and tracer transport. J. Contam. Hydrol. 104, 4–35.
Kouznetsov, M.Y., Roodsari, R., Pachepsky, Y.A., Shelton, D.R., Sadeghi, A.M., Shirmohammadi, A., Starr, J.L., 2007. Modeling manure-borne bromide and fecal coliform transport with runoff and infiltration at a hillslope. J. Environ. Manage. 84, 336–346.
LeGrand-Marcq, C., Laudelout, H., 1985. Longitudinal dispersion in a forest stream. J. Hydrol. 78, 317–324.
Lenhart, J.J., Saiers, J.E., 2003. Colloid mobilization in water-saturated porous media under transient chemical conditions. Environ. Sci. Technol. 37, 2780–2787.
Marquardt, D.W., 1963. An algorithm for least-squares estimation of nonlinear parameters. J. Soc. Ind. Appl. Math. 11, 431–441.

Mawdsley, J.L., Bardgett, R.D., Merry, R.J., Pain, B.F., Theodorou, M.K., 1995. Pathogens in livestock waste, their potential for movement through soil and environmental pollution. Appl. Soil Ecol. 2, 1–15.
Muirhead, R.W., Collins, R.P., Bremer, P.J., 2006. Interaction of *Escherichia coli* and soil particles in runoff. Appl. Environ. Microbiol. 72, 3406–3411.
Pachepsky, Y.A., Shelton, D.R., 2011. *Escherichia coli* and fecal coliforms in freshwater and estuarine sediments. Crit. Rev. Environ. Sci. Technol. 41, 1067–1110.
Pachepsky, Y.A., Sadeghi, A.M., Bradford, S.A., Shelton, D.R., Guber, A.K., Dao, T., 2006. Transport and fate of manure-borne pathogens: modeling perspective. Agric. Water Manage. 86, 81–92.
Pachepsky, Y., Shelton, D.R., McLain, J.E.T., Patel, J., Mandrell, R.E., 2011. Irrigation waters as a source of pathogenic microorganisms in produce: a review. Adv. Agron. 113, 73–138.
Panday, S., Huyakorn, P.S., 2004. A fully coupled physically-based spatially-distributed model for evaluating surface/subsurface flow. Adv. Water Resour. 27, 361–382.
Rahe, T., McCoy, C., Kling, E., 1978. Transport of antibiotic-resistant *Escherichia coli* through western Oregon hillslope soils under conditions of saturated flow. J. Environ. Qual. 7, 487.
Richards, L.A., 1931. Capillary conduction of liquids through porous media. Physics 1, 318–333.
Rijnaarts, H.H.M., Norde, W., Bouwer, E.J., Lyklema, J., Zehnder, A.J.B., 1995. Reversibility and mechanism of bacterial adhesion. Coll. Surf. B: Biointerf. 4, 5–22.
Runkel, R.L., Bencala, K.E., Broshears, R.E., Chapra, S.C., 1996. Reactive solute transport in streams: 1. Development of an equilibrium-based model. Water Resour. Res. 32, 409–418.
Šimůnek, J., van Genuchten, M.Th., 2008. Modeling nonequilibrium flow and transport processes using HYDRUS. Vadose Zone J. 7, 782–797.
Šimůnek, J., van Genuchten, M.Th., Šejna, M., 2008. Development and applications of the HYDRUS and STANMOD software packages and related codes. Vadose Zone J. 7, 587–600.
Šimůnek, J., van Genuchten, M.Th., Šejna, M., 2011. The HYDRUS Software Package for Simulating Two- and Three-Dimensional Movement of Water, Heat, and Multiple Solutes in Variably-Saturated Media, Technical Manual, Version 2.0, PC Progress, Prague, Czech Republic, pp. 258.
Tate, K.W., Pereira, M.D.G.C., Atwill, E.R., 2004. Efficacy of vegetated buffer strips for retaining Cryptosporidium parvum. J. Environ. Qual. 33, 2243–2251.
Thackston, E.L., Schnelle Jr., K.B., 1970. Predicting the effects of dead zones on stream mixing. J. Sanit. Eng. Div., Am. Soc. Civil Eng. 96 (SA2), 319–331.
Thompson, S.E., Katul, G.G., Porporato, A., 2010. Role of microtopography in rainfall-runoff partitioning: an analysis using idealized geometry. Water Resour. Res. 46, W07520.
Tosco, T., Tiraferri, A., Sethi, R., 2009. Ionic strength dependent transport of microparticles in saturated porous media: modeling mobilization and immobilization phenomena under transient chemical conditions. Environ. Sci. Technol. 43, 4425–4431.
Trask, J.R., Kalita, P.K., Kuhlenschmidt, M.S., Smith, R.D., Funk, T.L., 2004. Overland and near-surface transport of Cryptosporidium parvum from vegetated and nonvegetated surfaces. J. Environ. Qual. 33, 984–993.
Tufenkji, N., Dixon, D.R., Considine, R., Drummond, C.J., 2006. Multi-scale Cryptosporidium/sand interactions in water treatment. Water Res. 40, 3315–3331.
Tyrrel, S.F., Quinton, J.N., 2003. Overland flow transport of pathogens from agricultural land receiving faecal wastes. J. Appl. Microbiol. 94, 87–93.
USEPA, 1997. National Water Quality Inventory, Report to Congress. Rep. 841-R-97-008. USEPA, Washington, DC.
USFDA, 1998. Guidance for Industry: Guide to Minimize Microbial Food Safety Hazards for Fresh Fruits and Vegetables. Federal Register. October 29, 1998. p. 58055–58056.
van Genuchten, M.Th., Leij, F.J., Skaggs, T.H., Toride, N., Bradford, S.A., Pontedeiro, E.M., 2013. Exact analytical solutions for contaminant transport in rivers: 2. Transient storage and decay chain solutions. J. Hydrol. Hydromech. 61, 250–259.
Verwey, E.J.W., Overbeek, J.T.G., 1948. Theory of the Stability of Lyophobic Colloids. Elsevier, Amsterdam.
Wallach, R., van Genuchten, M.T., 1990. A physically based model for predicting solute transfer from soil solution to rainfall-induced runoff water. Water Resour. Res. 26, 2119–2126.
Wallach, R., Grigorin, G., Rivlin, J., 2001. A comprehensive mathematical model for transport of soil-dissolved chemicals by overland flow. J. Hydrol. 247, 85–99.
Weill, S., Mouche, E., Patin, J., 2009. A generalized Richards equation for surface/subsurface flow modelling. J. Hydrol. 366, 9–20.
Wörman, A., Packman, A.I., Marklund, L., Harvey, J.W., Stone, S.H., 2007. Fractal topography and subsurface water flows from fluvial bedforms to the continental shield. Geophys. Res. Lett. 34, L07402.
Wu, L., Gao, B., Munoz-Carpena, R., 2011. Experimental analysis of colloid capture by a cylindrical collector in laminar overland flow. Environ. Sci. Technol. 45, 7777–7784.
Yu, C., Gao, B., Muñoz-Carpena, R., Tian, Y., Wu, L., Perez-Ovilla, O., 2011. A laboratory study of colloid and solute transport in surface runoff on saturated soil. J. Hydrol. 402, 159–164.
Yu, C., Gao, B., Muñoz-Carpena, R., 2012. Effect of dense vegetation on colloid transport and removal in surface runoff. J. Hydrol. 434, 1–6.
Yu, C., Muñoz-Carpena, R., Gao, B., Perez-Ovilla, O., 2013. Effects of ionic strength, particle size, flow rate, and vegetation type on colloid transport through a dense vegetation saturated soil system: experiments and modeling. J. Hydrol. 499, 316–323.